Article

A Novel 2D DNA Nanoprobe Mediated Enzyme-free Target Recycling Amplification for Ultrasensitive Electrochemical Detection of MicroRNA

Xiaolong Zhang, Zhehan Yang, Yuanyuan Chang, Min Qing, Ruo Yuan, and Yaqin Chai

Anal. Chem., **Just Accepted Manuscript** • DOI: 10.1021/acs.analchem.8b02251 • Publication Date (Web): 09 Jul 2018

A Novel 2D DNA Nanoprobe Mediated Enzyme-free Target Recycling Amplification for Ultrasensitive Electrochemical Detection of MicroRNA

Xiaolong Zhang, Zhehan Yang, Yuanyuan Chang, Min Qing, Ruo Yuan*, Yaqin Chai*

Key Laboratory of Luminescence and Real-Time Analytical Chemistry (Southwest University), Ministry of Education, College of Chemistry and Chemical Engineering, Southwest University, Chongqing 400715, PR China

ABSTRACT

In the work, based on a new 2D DNA nanoprobe (DNP) and an enzyme-free target recycling amplification, an electrochemical biosensor is developed for the ultrasensitive detection of microRNA-21 (miRNA-21). Herein, the two ferrocene-labeled bipedal DNP which shows small steric hindrance and strong stability is prepared based on the mechanism of the proximity ligation assay (PLA), improving the space utilization. In the presence of the target miRNA-21 and a hairpin DNA strand, the DNP will be collapsed, and then two ferrocene-labeled DNA strands and the miRNA-21 will be simultaneously released from electrode surface through the toehold-mediated strand displacement reactions (TSDRs), leading to the decrease of electrochemical signal and realization of enzyme-free target recycling. As a result, the one input target miRNA-21 could release 2N multiple output ferrocene-labeled DNA strand, achieving dramatic decrease of the electrochemical signal. Combining DNP

* Corresponding author. Tel.: +86-23-68252277; Fax: +86-23-68253172.

E-mail address: yuanruo@swu.edu.cn(R.Yuan), yqchai@swu.edu.cn (Y. Q. Chai).

and the enzyme-free target recycling, this proposed biosensor showed a well linear dependence with the miRNA-21 communication range from 1.0 fM to 10 nM and a detection limit of 0.31 fM. In addition, it is worth mention that this biosensor can be regenerated through incubating with three assistant DNA strands, realizing the reuse of raw materials. Surprisingly, the elaborated biosensor provides a novel strategy for building controllable DNA nanoprobe for sensitive detection of various biomarkers.

INTRODUCTION

MicroRNA (miRNA) can act as both oncogenes and tumor suppressors, highlighting their importance in human cancer.[1, 2] In consequence, miRNA expression profiles can be regarded as the one of the biomarker for early diagnosis of different cancers.[3, 4] In order to achieve the aim to detect miRNA, many traditional available approaches such as bioluminescence assays,[5] Northern blotting[6-8] and quantitative RT-PCR (qRT-PCR)[9] are widely utilized. However, these methods are unsuitable in clinical analysis due to high-cost, time-consuming, complex and low sensitivity. Recently, some methods combining with rolling circle amplifications,[10, 11] nanomaterial[12] and nuclease-assisted target recycling[13] have received more attention for its significant signal enhancement capability. Among these new approaches, nuclease-assisted target recycling attracts a wide spread interests owing to the one-step, 1:N ratio pattern of target/probe molecular recognition and great signal amplified capability.[14] Nevertheless, poor stability and high cost of the nuclease hindered the versatile applications. Alternatively, the enzyme-free target recycling amplification based on target-catalyzed hairpin assembly and the toehold-mediated

strand displacement reactions (TSDRs) is developed in recent reported study.[15-19] However, the surface-induced perturbation of probes reduce accessibility of the target molecule to probes, which limits the efficiency of enzyme-free target recycling amplification.[20, 21] Thus, it is desirable to design a novel probe to recognize target molecule with high efficiency for achieving enzyme-free target recycling amplification.

DNA nanotechnology has attracted intense interest with highly programmable nature, high precision, and ease of preparation. As a result, various DNA nanostructures including 1-dimension (1D),[22] 2-dimension (2D)[23] and 3-dimension (3D)[20, 24-27] are designed. For instance, the tetrahedral DNA nanostructures (TDNs) as a typical 3D DNA nanostructure possess advantages of well controlled density, orientation of DNA bioprobes and minimized nonspecific adsorption on the surface.[20, 25] Nevertheless, the 3D mechanical rigidity of the TDNs results in higher steric effect on electrode. Although 1D DNA nanostructure possesses low steric hindrance, but the high surface-induced perturbation decrease immobilization efficiency on the electrode.[20, 28, 29] In light of above drawbacks, 2D DNA nanostructures with a dual-thiol labeling not only possess lower steric effect compared with 3D DNA nanostructures, but also overcome the shortcomings of nonspecific interaction and lower stability in contrast to 1D DNA nanostructures.[23] Recently, the proximity ligation assay (PLA) for the detection of protein has gained increasing interest, in which binding two affinity ligands to target protein can prevent spatial diffusion to close the complementary oligonucleotides proximity and dramatically increase their

local effective concentrations, thereby enhancing the efficiency and stability of the hybrids.[30, 31] Inspired by the mechanism, in this research, we aim to design a novel 2D DNA nanoprobe (DNP) with better flexibility, stability and buildability to improve the efficiency of enzyme-free target recycling amplification.

In the present work, an electrochemical biosensor based on the 2D DNA nanoprobe (DNP) and the enzyme-free target recycling amplification was prepared for the detection of microRNA-21. Briefly, as displayed in Scheme 1, with the help of single strand A1, the ferrocene-labeled A2 and A3 could be bring close proximity to hybridize with the surface-bound DNA strands (S1 and S2), making the ferrocene labels close to the electrode surface with obvious electrochemical response. With the involvement of target miRNA-21, the hairpin H could be opened to expose the prelocked toehold domain for the hybridization of A1. Finally, based on the toehold-mediated strand displacement reactions (TSDRs), the hybridization of H and A1 caused ferrocene-labeled A2 and A3 away from the electrode, accompanying with the release of target miRNA-21. Since the liberated target opened hairpin H for triggering another TSDRs, a large number of ferrocene-labeled DNA were released from electrode, resulting dramatic decrease of electrochemical response. As a result, the one input of target can induce 2N multiple output ferrocene-labeled DNA strands released from the electrode surface. Additionally, this biosensor could be regenerated, realizing the reuse of raw materials. Thus, this strategy provided a novel avenue for detecting various nucleic acid in nascent stage of cancer.

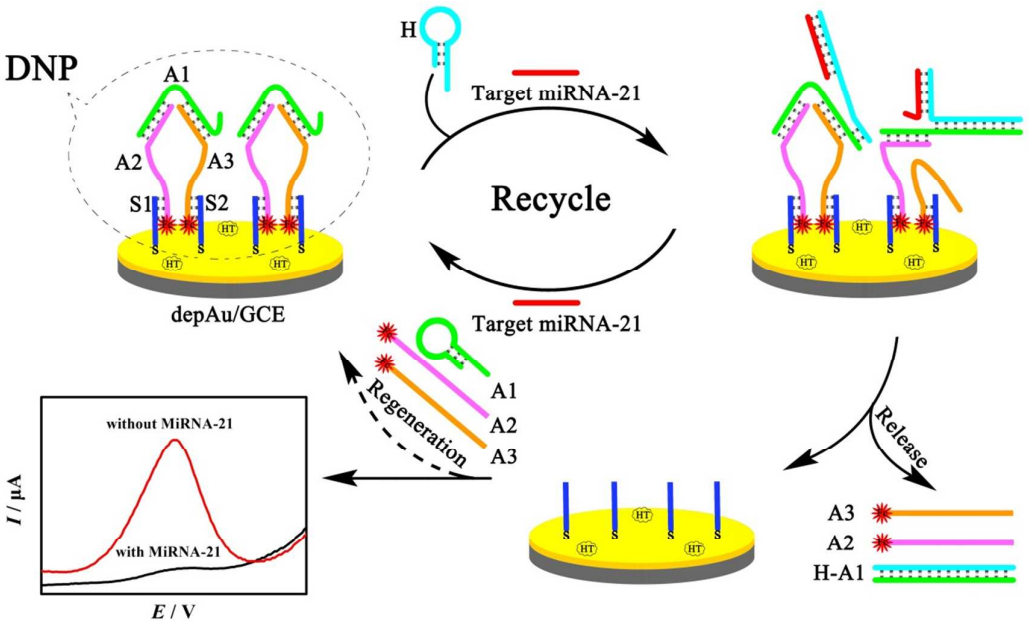

Scheme 1. Schematic illustration of the biosensor based on the 2D DNA nanoprobe (DNP) and the enzyme-free target recycling amplification for the miRNA-21 assay.

EXPERIMENT SECTION

Chemical and Materials Gold chloride ($HAuCl_4 \cdot 4H_2O$), Hexanethiol (HT) and Tris (2-carboxyethy) phosphine hydrochloride (TCEP) were purchased from Sigma (St. Louis, MO, USA). The HPLC-purified oligonucleotides were supplied by Sangon Inc. (Shanghai, China), and Table 1 showed the sequences of the oligonucleotides used in the experiment. Tris-HCl buffer (20 mM Tris, 140 mM NaCl, 1.0 mM $MgCl_2$, 5 mM Cl, 1.0 mM $CaCl_2$, pH 7.4) was used to dilute oligonucleotides. 5xTBE buffer (250 mM Tris, 250 mM H_3BO_3, 10 mM EDTA, pH 8.0) was applied to perform polyacrylamide gel electrophoresis (PAGE) experiment. Phosphate buffered solution (PBS) buffer (100 mM Na_2HPO_4, 100 mM KH_2PO_4, 100 mM KCl, pH 7.0) and $[Fe(CN)_6]^{3-/4-}$ solution (20 mM Tris-HCl, 5 mM $K_3[Fe(CN)_6]$, 5 mM $K_4[Fe(CN)_6]$, pH 7.4) were prepared to carry out the performance measurements of the biosensor.

Table 1. Synthetic oligonucleotide sequences

sequence	from 5' to 3'
H	ATCAGACTGTGGACTAAGGCTCAACATCAGTCTGATAAGCTA
A1	TAGCTTATCAGACTGATGTTGAGCCTTAGTCCACAGTCTGAT
A2	CAGTCTGATAAGCTATTTTTTTTTTTTTTTTTTGGGTTAGGG-Fc
A3	Fc-GGGATTGGGTTTTTTTTTTTTTTTTTCTGTGGACTAAGGCT
A2'	CATCAGTCTGATAAGCTATTTTTTTTTTTTTTTTTTGGGTTAGGG-Fc
A3'	Fc-GGGATTGGGTTTTTTTTTTTTTTTTTCTGTGGACTAAGGCTCAA
S1	SH-$(CH_2)_6$-TTTTTTCCCTAACCC
S2	CCCAATCCCTTTTTT-$(CH_2)_6$-SH
miRNA-21	UAGCUUAUCAGACUGAUGUUGA
miRNA-141	UAACACUGUCUGGUAAAGAUGG
miRNA-155	UUAAUGCUAAUCGUG AUAGGGGU
let-7a	UGAGGUAGUAGGUUGUAUAGUU

Apparatus and Measurements. Cyclic Voltammetry (CV), Electrochemical Impedance Spectroscopy (EIS) and Differential Pulse Voltammetry (DPV) were accomplished by using a CHI 660D electrochemical workstation (CH Instruments, Shanghai, China) with a three-electrode arrangement. Polyacrylamide Gel Electrophoresis (PAGE) was conducted by a Bio-Rad imaging system (Hercules, CA, USA). The CV and EIS signal of the sensor establishment were processed in 2 mL 5 mM $[Fe(CN)_6]^{3-/4-}$ solution with a scanning potential from -0.2 V to 0.6 V (scan rate 100 mV/s). And the DPV was conducted in 0.1 M PBS (pH 7.0) with the potential

from 0.2 V to 0.7 V (pulse amplitude 20 mV, pulse width 50 ms, and pulse period 0.2 s), which was used to evaluate the electrochemical performance of the developed biosensor under the optimal experimental conditions.

Fabrication of Biosensor. First of all, the bare glassy carbon electrode (GCE) was polished carefully with alumina slurry (0.3 μm and 0.05 μm) followed by ultrasonic treatment with ethanol and distilled water, respectively. After that, the electrode was immersed into $HAuCl_4$ aqueous solution (1%) and electrodeposited at -0.2 V for 30 s to coat a layer of gold particles (depAu).

Subsequently, 10 μL of Tris-HCl (pH 7.4) including S1 (1.0 μM) and S2 (1.0 μM) was dropped onto the surface of electrode (depAu/GCE) and incubated for 12 h at room temperature. After rinsing with buffer for removing the nonspecifically adsorbed DNA, the electrode was incubated with HT (1 mM) for 30 min to block the active sites of electrode.

Finally, 10 μL of 1.0 μM A1 was heated to 90 ^{o}C for 10 min and cooled down to room temperature for at least 1h to form the hairpin DNA. Then, 10 μL of the mixture of A1 (1.0 μM), A2 (1.0 μM) and A3 (1.0 μM) was added onto the above electrode (HT/S1-S2/depAu/GCE) and incubated at 37 ^{o}C (Figure S1A) to obtain the DNA nanoprobe (DNP).

For detection of target miRNA-21, the 10 μL of mixture containing annealed hairpin DNA (H, 1.0 μM) and various concentration of target miRNA-21 was dropped onto the electrode (HT/probe/depAu/GCE) and incubated at 40 ^{o}C. After washing with buffer, the biosensor was performed by electrochemical characterization.

Additionally, the regeneration of biosensor was achieved by incubating with the mixture of A1 (1.0 μM), A2 (1.0 μM) and A3 (1.0 μM).

Polyacrylamide Gel Electrophoresis (PAGE). After the DNA samples were mixed with DNA loading buffer (volume ratio 5:1), the dynamic DNA assemble products were analyzed by the freshly prepared 16 % polyacrylamide gel electrophoresis (PAGE) in 1xTBE buffer (pH 8.0) at 120 V for 120 min.

RESULTS AND DISCUSSION

Polyacrylamide Gel Electrophoresis (PAGE) Analysis. The reaction mechanism of TSDRs was verified by PAGE. AS shown in Figure 1. The obvious bands in Lane 1, lane 2, lane 3, lane 4 and lane 5 correspond to the miRNA-21, A2, A3, A1, and H, respectively. After the hairpin H mixed with the miRNA-21 (lane 6), a strong band with slow migration (the top band in lane 6) could be noticed, suggesting the successful hybridization of H and miRNA-21. Lane 7 corresponded to the three-strand DNA duplex consisting of strands A1, A2, and A3. When the three-strand DNA duplex of A1, A2 and A3 was mixed with the DNA duplex of hairpin H and miRNA-21, an additional band (the middle band in lane 8) corresponding to the DNA duplex from the hybridization of H and A1 was appeared in comparison with lane 6 and lane 7, further indicating the happening of the TSDRs between these two DNA duplexes. These observations strongly indicated that the DNP could be used for the detection of miRNA-21.

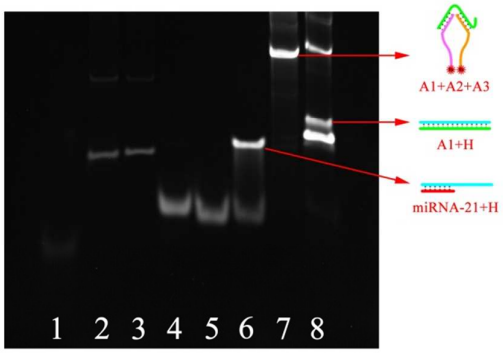

Figure 1. Nondenaturing PAGE analysis : lane 1, miRNA-21 (4 μM); Lane 2, A2 (2 μM); Lane 3, A3 (2 μM); Lane 4, hairpin A1 (2 μM); Lane 5, hairpin H (2 μM); Lane 6, microRNA-21 (2 μM) and hairpin H (2 μM); Lane 7, A1 (2 μM), A2 (2 μM), A3 (2 μM); Lane 8, A1 (2 μM), A2 (2 μM), A3 (2 μM) and microRNA-21 (2 μM), hairpin H (2 μM).

Electrochemical Characterization of the Biosensor. The stepwise fabrication of the biosensor was characterized by CV and EIS. As shown in Figure 2A (CV), a pair of well-defined redox peaks (curve a) could be noticed for the bare GCE, When the AuNPs were electrodeposited onto the GCE, the redox currents increased (curve b) resulting of the excellent conductivity of AuNPs. Afterwards, the redox–currents obviously decreased (curve c) with the immobilization of S1 and S2 on the electrode, which could be attributed to the repulsion effect between the $[Fe(CN)_6]^{3-/4-}$ and negatively charged phosphate backbone of DNA. Then, with the self-assembly of HT on the electrode, the redox currents further decreased (curve d). Subsequent assembling of DNP caused dramatic decrease of redox currents (curve e), because more negative charge was carried onto the electrode surface.

And as shown in Figure 2B (EIS), we can find a small semicircle diameter and a long tail denoting diffusion showing the well conductivity of the bare GCE (curve a).

When the depAu with large surface area and excellent conductivity were electrodeposited onto the bare GCE, a straight line could be found (curve b). Subsequently, with more DNA strands and HT incubated onto the electrode, an obvious increasing trend of R_{et} (curve c, curve d, curve e) could be observed owing to the enhanced steric hindrance from the stack of DNA strands and HT which could result in the dramatically decreased conductivity of the electrode. These results were consistent with that observed in CV, demonstrating the biosensor was successfully assembled.

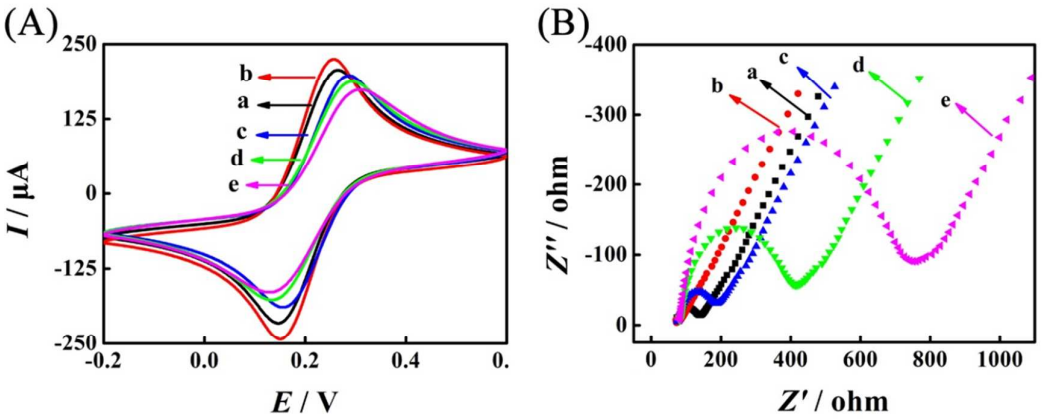

Figure 2. (A) Typical CV responses and (B) EIS responses of different modified electrodes: (a) bare GCE, (b) depAu/GCE, (c) S1-S2/depAu/GCE, (d) HT/S1-S2/depAu/GCE, (e) A1-A2-A3/HT/S1-S2/depAu/GCE.

Comparison of Current Response of Biosensor with Different Modifications. In order to verify that the free domain in the middle of A1 could improve the immobilization efficiency of DNP (Figure 3A, a), we designed another 2D DNA nanoprobe (DNP′) (Figure 3A, b) by increasing the hybridization sequence of A2 and A3 to block the free domain of A1 for the comparison of their electrochemical responses. As shown in Figure 3B, under optimal conditions (Figure S1), the current

response of DNP (curve a) was almost twice as much as the current response of DNP′ (curve b), which might be the result of the fact that the better flexibility of DNP endowed it with lower steric hindrance for enhancing the immobilization efficiency. Moreover, the results above also indicated the excellent performance of the DNP.

To certify that the PLA could induce the close proximity of ferrocene-labeled DNAs (A2, A3) by A1 for increasing the current response in this work, we adopted DPV to investigate the electrochemical signal of the proposed biosensor with or without A1 for constructing DNP (Figure 3C). Since two ferrocene-labeled DNAs (A2 and A3) were unable to hybridize with S1 and S2 without the A1, no DPV current response (curve b) was observed. Once the A1 was introduced in this system for the formation of DNP with the help of A2 and A3, an obvious current response (curve a) was observed, indicating that the PLA-triggered by A1 could indeed bring into close proximity of ferrocene-labeled DNAs (A2 and A3) for enhancing the electrochemical signal.

To further verify the introduction of TSDRs could efficiently achieve the miRNA-21 detection, the proposed biosensor was investigated by DPV. As displayed in Figure 3D, compared with the current response of the biosensor incubated with DNP (curve a), the biosensor incubated with either the target miRNA-21 (curve b) or the hairpin H (curve c) alone presented ignorable current changes. However, in the presence of both target miRNA and H, an obvious decrease in the DPV current response was observed (curve d), suggesting that the TSDRs triggered by miRNA-21, H and DNP could cause ferrocene-labeled A2 and A3 away from the electrode surface.

These results exhibited that the TSDRs played an essential role in the detection of miRNA-21.

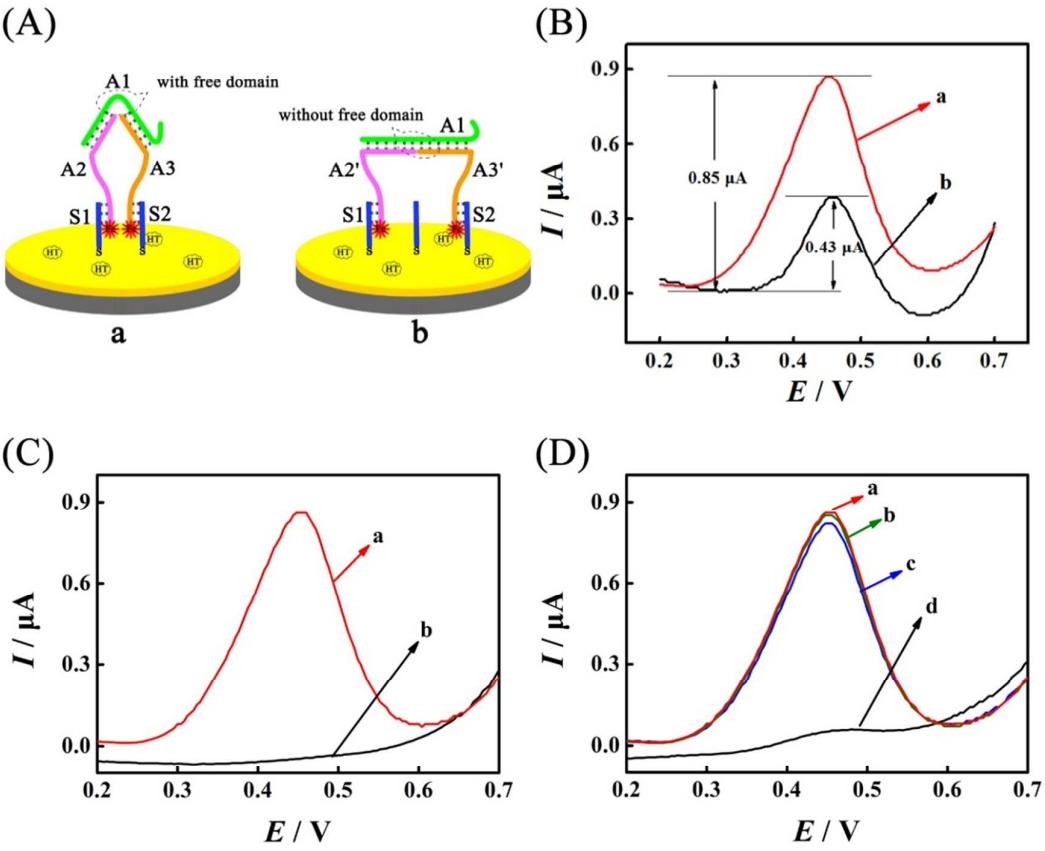

Figure 3. (A) Schematic illustration for (a) DNP and (b) DNP′. Comparison of the DPV responses of (B) (a) DNP and (b) DNP′ under the optimal condition, (C) the biosensor when DNP was constructed (a) with A1 and (b) without A1, and (D) (a) the biosensor prepared, (b) (a) incubated with H, (c) (a) incubated with miRNA-21, (d) (a) incubated with both miRNA-21 and H.

Performance of the Biosensor. Under the optimal experimental conditions (Figure S1), the sensing platform was incubated with different concentrations of miRNA-21 and evaluated by DPV. As displayed in Figure 4A, the DPV current response gradually decreased with the elevated concentration of target from 1.0 fM to 10 nM, and showed an excellent linear relationship with the logarithm of the

miRNA-21 concentration. The corresponding calibration plot was illustrated in Figure 4B, and the regression equation was expressed as I = -0.09719 lg c -0.71918 (I is the peak current and c is the target miRNA-21 concentration) with the correlation coefficient value (R) of -0.9987. Moreover, a detection limit of 0.31 fM for miRNA-21 detection could be calculated according to the 3σ rule. Significantly, compared to other biosensors, as shown in Table 2, the proposed biosensor had an attractive wider linear range and relative lower detection limit, which could be owing to the synergistic effect of the high immobilization efficiency of DNP and the high reaction efficiency of TSDRs.

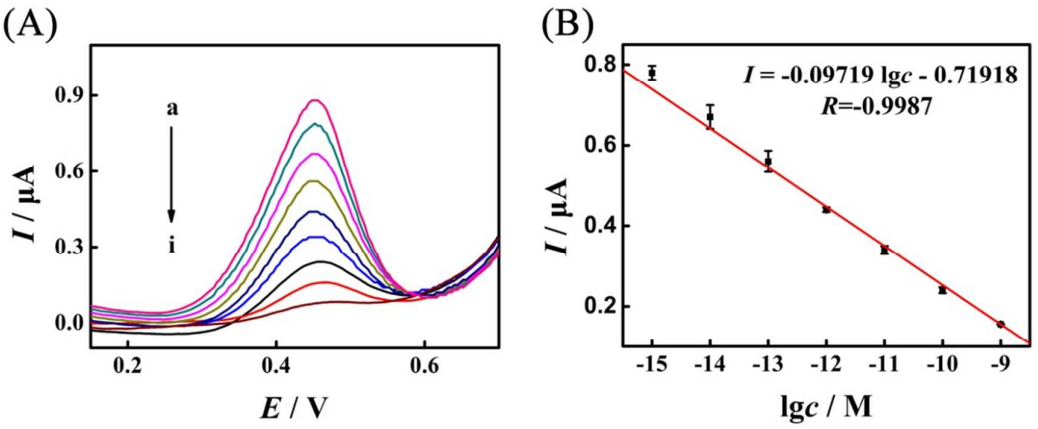

Figure 4. (A) DPV current responses of the biosensors to different concentration of the target miRNA-21. From a to i: 0 fM, 1.0 fM, 10 fM, 100 fM, 1.0 pM, 10 pM, 100 pM, 1.0 nM, and 10 nM (a to i). (B) The corresponding calibration plot for the DPV peak current *vs* lg c.

Table 2. Comparison of the proposed biosensor with other miRNA detection strategies

analytical methods	linear range	detection limit	ref
surface-enhanced Raman scattering	10 fM to 100 pM	10 fM	32
electrochemiluminescence	5.0 fM to 500 pM	1.51 fM	33
fluorescence	100 fM to 10 nM	58 fM	34
chronocoulometry	2.0 fM to 1.0 nM	2.0 fM	35
square wave voltammetry	5.0 fM to 50 pM	3.0 fM	36
differential pulse voltammetry	1.0 pM to 800 pM	1.0 pM	37
differential pulse voltammetry	10 fM to 100.0 nM	1.2 fM	38
differential pulse voltammetry	5 fM to 5.0 pM	1.92 fM	39
differential pulse voltammetry	1.0 fM to 10 nM	0.31 fM	this work

Reproducibility, Selectivity, and Stability of the Biosensor. To investigate the reproducibility, six repetitive measurements for the target miRNA-21 at 0.1 nM was studied and the relative standard deviations (RSDs) were 5.1%, suggesting the acceptable reproducibility of this biosensor. Additionally, to investigate the specificity of this developed biosensor, three different miRNA sequences (miRNA-141, miRNA-155 and let-7a) and specific protein thrombin were selected as the possible interfering substances of target miRNA-21. As shown in Figure 5A, no significant

change in the current response was noticed in the presence of the non-target substances. However, even with 100-fold lower miRNA-21 (0.1 nM), the change of current response was much larger than that of non-target substances. Additionally, when 0.1 nM miRNA-21 was mixed with the aforementioned three different miRNA sequences, the current response was almost the same as the value obtained from miRNA-21 only. The results suggested the satisfactory selectivity of the proposed biosensor. Moreover, the long-term stability experiment was investigated by storing the proposed biosensor at 4 °C and measuring every 5 days (Figure 5B). After a longer storage for 20 days, no significant change was found in DPV and the current response maintained 91.3% of the initial one. The results illustrated that the prepared biosensor exhibited satisfactory stability.

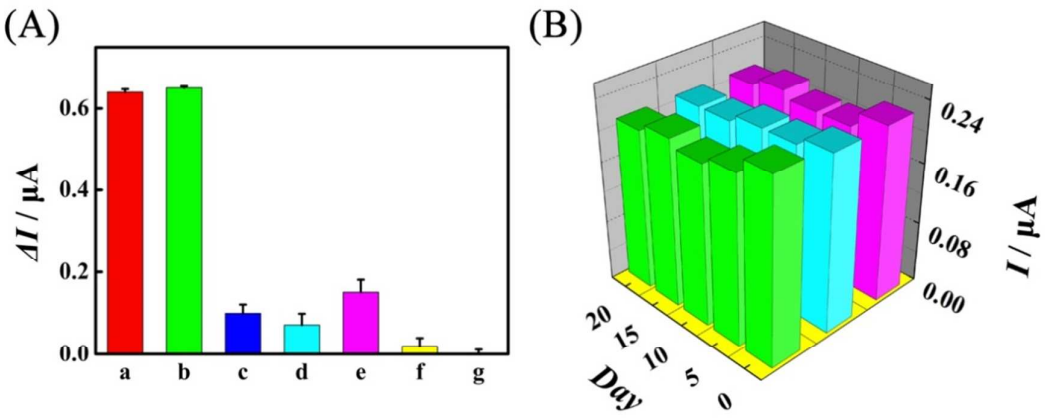

Figure 5. (A) The specificity of the electrochemical biosensor: (a) miRNA-21 (0.1 nM), (b) mixed sample (c) miRNA-141 (10 nM), (d) miRNA-155 (10 nM), (e) thrombin (10 nM), (f) let-7a (10 nM), (g) blank sample; (B) the stability of the proposed biosensor (miRNA-21 0.1 nM).

Regeneration Ability of the Biosensor. The biosensor regeneration was realized by incubating another three DNA strands of A1, A2 and A3 on the electrode after the

DNP was collapsed. As shown in Figure 6A, after the miRNA-21 detection took place, no obvious DPV response of electroactive material ferrocene was presented (curve b); when the A1, A2 and A3 were captured on the electrode, the electrochemical response (curve c) which is similar to that of the initial biosensor (curve a) appeared, indicating the successful regeneration of the constructed biosensor. Moreover, the proposed biosensor was regenerated for 4 times with the regeneration rate range from 92.67% to 101.93% (Figure 6B), which further proved the well regeneration ability of the biosensor and illustrated that the biosensor could be potentially reused for many times.

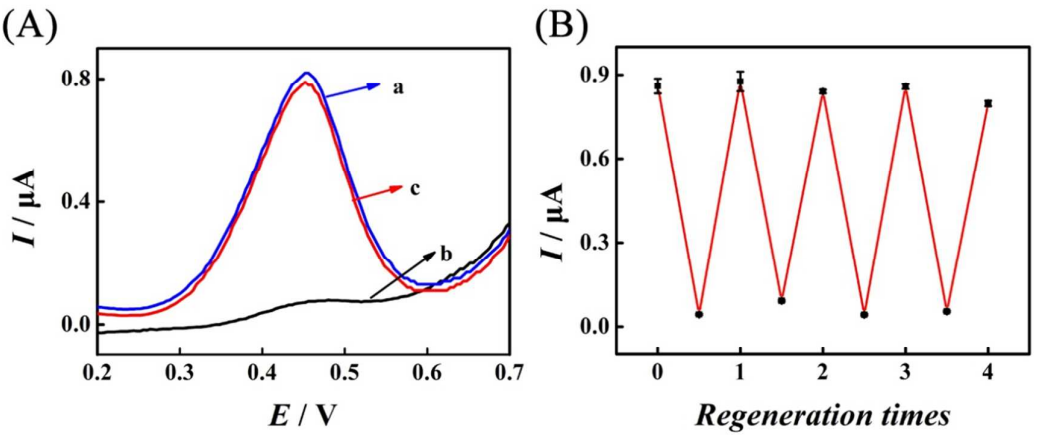

Figure 6. (A) DPVs of (a) before and (b) after the prepared biosensor underwent miRNA-21 detection; (c) the regeneration of the biosensor one time. (B) regeneration of the biosensor for miRNA-21 detection with 4 times under the same condition.

Real Application of the Biosensor in Cancer Cells. To investigate the capacity of the proposed biosensor, the detection for real samples was carried out by monitoring miRNA-21 in the lysates from human cancer cells of breast (MCF-7) and cervical (Hela). As the results displayed in Figure 7, with the increase of the cell

numbers, the change of DPV response gradually increased, indicating the high expression of miRNA-21 in MCF-7 cells. While no obvious DPV response change was observed, indicating a low expression of miRNA-21 in Hela cells. These results from this study was in accordance with previous researches,[40-42] suggesting that the elaborated biosensor could be applied to monitor the miRNA biomarkers expression from the cancer cells.

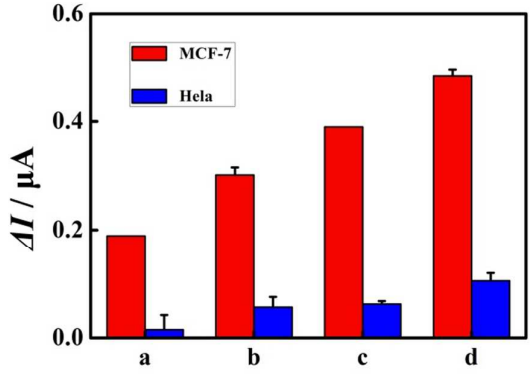

Figure 7. Data analysis of the proposed biosensor from different cancer cell lysates: (a) MCF-7 (10 cells) and Hela (10 cells), (b) MCF-7 (100 cells) and Hela (100 cells), (c) MCF-7 (1000 cells) and Hela (1000 cells), (d) MCF-7 (10000 cells) and Hela (10000 cells).

CONCLUSION

In summary, we have successfully demonstrated an electrochemical biosensing platform using a novel bipedal 2D DNA nanoprobe (DNP) to ultrasensitively detect miRNA. This study presented three novel ideas as follows. First, the special design of bipedal DNP possessed excellent flexibility and stability that could improve immobilization efficiency and enhance electrochemical signal response, resulting in improved detection sensitivity. Meanwhile, the DNP constructed by high-efficiency PLA could be reconstructed through a one-step incubation of three DNA strands,

which endowed the biosensor with well regeneration ability to effectively low the experiment cost, and the regeneration rate ranged from 92.67% to 101.93% over 4 times. Finally, the introduction of the enzyme-free target recycling amplification further successfully enhanced the detection sensitivity and realized the ultrasensitive analysis of miRNA-21. Overall, the proposed biosensor exhibited good sensitivity, stability and specificity, and provided a novel strategy based on the 2D DNA nanoprobe for the biosensor construction, which could be generalized to many other biomarkers analysis.

ASSOCIATED CONTENT

Supporting information

Figure S1 showed the Optimization of Experimental Conditions.

ACKNOWLEDGMENTS

This paper was financially supported by the National Natural Science Foundation of China (51473136, 21675129, 21575116 and 21775124) and the Fundamental Research Funds for the Central Universities (XDJK2017A001, XDJK2018AA003), China.

REFERENCES

(1) Johnson, S. M.; Grosshans, H.; Shingara, J.; Byrom, M.; Jarvis, R.; Cheng, A.; Labourier, E.; Reinert, K. L.; Brown, D.; Slack, F. J. *Cell* **2005**, *120*, 635-647.

(2) Stahlhut Espinosa, C. E.; Slack, F. J. *J. Biol. Med.* **2006**, *79*, 131-141.

(3) Kosaka, N.; Iguchi, H.; Ochiya, T. *Cancer Sci.* **2010**, *101*, 2087-2092.

(4) Tricoli, J. V.; Jacobson, J. W. *Cancer Res.* **2007**, *67*, 4553.

(5) Cissell, K. A.; Rahimi, Y.; Shrestha, S.; Hunt, E. A.; Deo, S. K. *Anal. Chem.* **2008**, *80*, 2319-2325.

(6) Ruby, J. G.; Jan, C.; Player, C.; Axtell, M. J.; Lee, W.; Nusbaum, C.; Ge, H.; Bartel, D. P. *Cell* **2006**, *127*, 1193-1207.

(7) Válóczi, A.; Hornyik, C.; Varga, N.; Burgyán, J.; Kauppinen, S.; Havelda, Z. *Nucleic Acids Res.* **2004**, *32*, e175.

(8) Berezikov, E.; Thuemmler, F.; Van Laake, L. W.; Kondova, I.; Bontrop, R.; Cuppen, E.; Plasterk, R. H. A. *Nat. Genet.* **2006**, *38*, 1375-1377.

(9) Kulcheski, F. R.; Marcelino-Guimaraes, F. C.; Nepomuceno, A. L.; Abdelnoor, R. V.; Margis, R. *Anal. Biochem.* **2010**, *406*, 185-192.

(10) Wen, Y.; Xu, Y.; Mao, X.; Wei, Y.; Song, H.; Chen, N.; Huang, Q.; Fan, C.; Li, D. *Anal. Chem.* **2012**, *84*, 7664-7669.

(11) Cheng, Y.; Zhang, X.; Li, Z.; Jiao, X.; Wang, Y.; Zhang, Y. *Angew. Chem. Int. Ed.* **2009**, *48*, 3268-3272.

(12) Polsky, R.; Gill, R.; Kaganovsky, L.; Willner, I. *Anal. Chem.* **2006**, *78*, 2268-2271.

(13) Yu, Y.; Chen, Z.; Shi, L.; Yang, F.; Pan, J.; Zhang, B.; Sun, D. *Anal. Chem.* **2014**, *86*, 8200-8205.

(14) Yin, B. C.; Liu, Y. Q.; Ye, B. C. *J. Am. Chem. Soc.* **2012**, *134*, 5064-5067.

(15) Zhang, D. Y.; Winfree, E. *J. Am. Chem. Soc.* **2009**, *131*, 17303-17314.

(16) Green, S. J.; Lubrich, D.; Turberfield, A. J. *Biophys. J.* **2006**, *91*, 2966-2975.

(17) Huang, J. H.; Su, X. F.; Li, Z. G. *Anal. Chem.* **2012**, *84*, 5939-5943.

(18) Liu, S.; Wang, Y.; Ming, J.; Lin, Y.; Cheng, C.; Li, F. *Biosens. Bioelectron.* **2013**, *49*,

472-477.

(19) Yurke, B.; Jr, A. P. M. *Genet. Prog. Evol. Mach.* **2003**, *4*, 111-122.

(20) Wen, Y. L.; Pei, H.; Wan, Y.; Su, Y.; Huang, Q.; Song, S. P.; Fan, C. H. *Anal. Chem.* **2011**, *83*, 7418-7423.

(21) Zhu, D.; Pei, H.; Chao, J.; Su, S.; Aldalbahi, A.; Rahaman, M.; Wang, L.; Wang, L.; Huang, W.; Fan, C. *Nanoscale* **2015**, *7*, 18671-18676.

(22) Shi, K.; Dou, B. T.; Yang, C. Y.; Chai, Y. Q.; Yuan, R.; Xiang, Y. *Anal. Chem.* **2015**, *87*, 8578-8583.

(23) Li, C.; Wu, D.; Hu, X. L.; Xiang, Y.; Shu, Y. Q.; Li, G. X. *Anal. Chem.* **2016**, *88*, 7583-7590.

(24) Pei, H.; Lu, N.; Wen, Y.; Song, S.; Liu, Y.; Yan, H.; Fan, C. *Adv. Mater.* **2010**, *22*, 4659.

(25) Lu, N.; Pei, H.; Ge, Z.; Simmons, C. R.; Yan, H.; Fan, C. *J. Am. Chem. Soc.* **2012**, *134*, 13148-13151.

(26) Shen, W.; Zhong, H.; Neff, D.; Norton, M. L. *J. Am. Chem. Soc.* **2009**, *131*, 6660-6661.

(27) Pei, H.; Liang, L.; Yao, G.; Li, J.; Huang, Q.; Fan, C. *Angew. Chem. Int. Ed.* **2012**, *124*, 9154-9158.

(28) Zhu, D.; Song, P.; Shen, J. W.; Su, S.; Chao, J.; Aldalbahi, A.; Zhou, Z.; Song, S. P.; Fan, C. H.; Zuo, X. L.; Tian, Y.; Wang, L. H.; Pei, H. *Anal. Chem.* **2016**, *88*, 4949-4954.

(29) Lin, M. H.; Wang, J. J.; Zhou, G. B.; Wang, J. B.; Wu, N.; Lu, J. X.; Gao, J. M.; Chen, X. Q.; Shi, J. Y.; Zuo, X. L.; Fan, C. H. *Angew. Chem. Int. Ed.* **2015**, *54*, 2151-2155.

(30) Fredriksson, S.; Gullberg, M.; Jarvius, J.; Olsson, C.; Pietras, K.; Östman, A.; Landegren, U. *Nat. Biotechnol.* **2002**, *20*, 473-477.

(31) Schallmeiner, E.; Oksanen, E.; Ericsson, O.; Spångberg, L.; Eriksson, S.; Stenman, U. H.;

Pettersson, K.; Landegren, U. *Nat. Methods* **2007**, *4*, 135-137.

(32) Su, J.; Wang, D. F.; Nörbel, L.; Shen, J. L.; Zhao, Z. H.; Dou, Y. Z.; Peng, T. H.; Shi, J.; Mathur, S.; Fan, C. H.; Song, S. P. *Anal. Chem.* **2017**, *89*, 2531-2538.

(33) Peng, L. C.; Zhang, P.; Chai, Y. Q.; Yuan, R. *Anal. Chem.* **2017**, *89*, 5036-5042.

(34) Wang, L. D.; Deng, R. J.; Li, J. H. *Chem. Sci.* **2015**, *6*, 6777-6782.

(35) Fang, C. S.; Kim, K.; Yu, B.; Jon, S.; Kim, M.; Yang, H. *Anal. Chem.* **2017**, *89*, 2024-2031.

(36) Yang, C. Y.; Dou, B. T.; Shi, K.; Chai, Y. Q.; Xiang, Y.; Yuan, R. *Anal. Chem.* **2014**, *86*, 11913-11918.

(37) Hou, T.; Li, W.; Liu, X.; Li, F. *Anal. Chem.* **2015**, *87*, 11368-11374.

(38) Tian, Q. Q.; Wang, Y.; Deng, R. J.; Lin, L.; Liu, Y.; Li, J. H. *Nanoscale* 2015, 7, 987−993.

(39) Zhang, K.; Dong, H. F.; Dai, W. H.; Meng, X. D.; Lu, H. T.; Wu, T. T.; Zhang, X. J. *Anal. Chem*. 2016, 89, 648-655.

(40) Lu, J.; Tsourkas, A. *Nucleic Acids Res*. **2009**, *37*, e100.

(41) Si, M. L.; Zhu, S.; Wu, H.; Lu, Z.; Wu, F.; Mo, Y.-Y. *Oncogene* 2007, 26, 2799−2803.

(42) Selcuklu, S. D.; Donoghue, M. T. A.; Spillane, C. *Biochem. Soc. Trans*. 2009, 37, 918−925.

For TOC only

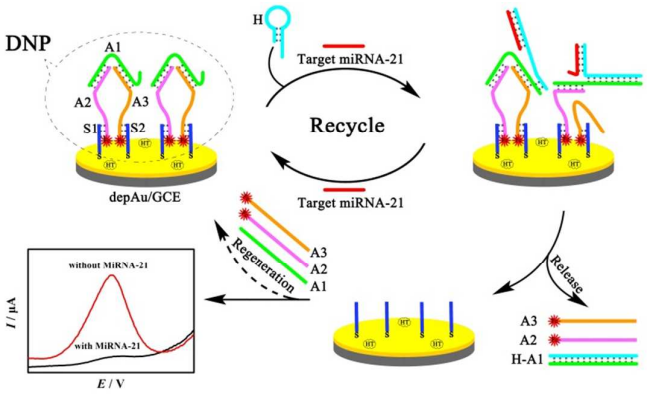
DNP
A1
A2
A3
S1
S2
depAu/GCE
H
Target miRNA-21
Recycle
Target miRNA-21
Regeneration
A3
A2
A1
Release
A3
A2
H-A1
without MiRNA-21
with MiRNA-21
I / μA
E / V